Reprinted from TEXTILE RESEARCH JOURNAL, Vol. 67, No. 12, December 1997
Printed in U.S.A.

Micromechanics of a Planar Hybrid Fibrous Network[1]

NING PAN,[2] JULIE CHEN,[3] MOON SEO,[4] AND STANLEY BACKER

Department of Mechanical Engineering, Massachusetts Institute of Technology, Cambridge, Massachusetts 02139, U.S.A.

ABSTRACT

A micromechanical approach is proposed in this work to predict the initial tensile response under uniaxial loading of a bonded two-dimensional fibrous network consisting of two kinds of fibers. The probabilities and statistical distributions of the hybrid bonding points and free fiber lengths between the bonding points in the structure are first derived, and the deformations of both the fiber segment and the bonding area of a typical microelement of the network are analyzed and calculated. The analysis of an arbitrary microelement is then extended statistically to an intermediate level of the structure, the mesodomain, through which the macroscopic deformations of the structure are computed. Ultimately, the general expressions of elastic moduli and Poisson's ratios for a hybrid fibrous network are obtained. A parametric study examines the relationships between fiber mechanical and dimensional properties, fiber volume fractions of the two fiber types, fiber orientation distributions and the properties of the bonding areas, and the tensile behavior of the structure for an ideal planar fiber network.

Many fibrous products such as papers made from pulped wood fibers and thin nonwoven materials can be considered planar structures of laid fiber networks. During manufacturing of these products, fibers are randomly dispersed throughout the suspension and bonded through various means to each other at intervals along their lengths to form the structure. Although the fibers are not strictly randomly distributed within the system due to the interactions among themselves and also to the machine flow direction speed during the fiber suspension process, a random orientation representation of the fibers or an isotropic assumption of the system is considered an acceptable approximation [8].

As to the assumption of such a fibrous structure as a two-dimensional planar network, Kallmes [8] stated that "there is relatively little interweaving among them (fibers), and most of their deviations out of the plane of the sheet are to accommodate adjacent fibers. Thus, the two dimensional model of paper is adequate for most, though by no means all, purposes."

Of all the attributes of the fibrous products, the mechanical properties are essential in determining their performance and applications. Unlike clothing materials, which usually encounter moderate mechanical actions during wearing, products like nonwoven geotextiles are under much higher loading conditions in service, so that high mechanical durability and other relevant properties are vital for their serviceability.

These products' mechanical properties are also important because they relate to the processibility of the products, *i.e.,* they have to be strong enough to cope with all the loads exerted on them during manufacturing. Because of the high speed and continuous nature of these processes, any breakage of the fiber web will severely impair the efficiency of the production.

There have already been various analytic attempts to study the planar fibrous network. The generally acknowledged pioneer in this area is Cox. In his report [6], he tried to predict the elastic behavior of paper based on the distribution and mechanical properties of the constituent fibers. Kallmes, Perkins, and Page contributed a great deal to this field through their research work on paper properties. In a series of reports, Kallmes and his colleagues [5, 8, 9, 10, 11] extended Cox's analysis by using probability theory to study fiber bonding points, the free fiber lengths between the contacts, and their distributions. Nissan [17] investigated the nature and strength of the bonding points. Schulgasser [29], Rigdahl *et al.* [28], and Page and his coworkers [18, 19, 20, 21, 30] considered the effects of fiber and bond properties on paper sheet performance. Perkins and Ramasubramanian [24, 25, 27] applied mi-

[1] This paper was presented at the INDA Fundamental Research Conference, Raleigh, North Carolina, July 21–22, 1992.

[2] Present address: Division of Textiles and Clothing and Biological and Agricultural Engineering Department, University of California, Davis, CA 95616.

[3] Present address: Department of Aerospace & Mechanical Engineering, Boston University, Boston, MA 02215.

[4] Present address: Kunkuk University, Seoul, Korea.

cromechanics to paper sheet analysis. Parallel to these studies on paper sheets, articles by Komori and Makishima [12, 13, 14], Chen and Duckett [4], Lee and Lee [15, 16], and Carnaby and Pan [3, 22, 23] dealt, in a broader perspective, with the microstructural characteristics and micromechanical analysis of general fibrous assemblies.

The major issue in dealing with the mechanical properties of any material is the formulation of stress and strain, the constitutive relations that govern the mechanical response of the material in question. For porous media such as fibrous materials, however, the traditional continuum approach is often inadequate if one intends to include the effects of the internal structure in order to better understand the mechanisms involved so as to modify the structure or more accurately predict the behavior of the material. Alternatives to continuum analyses are micromechanical analyses or, as more often used, the combination of micromechanics with continuum theory [1, 2].

The mechanical properties of these porous fibrous structures depend on the constituent fiber properties and the total number of fiber-fiber bonds, as well as the number of bonds per fiber, whereas the number and distribution of the bonding points are determined by the orientation and volume proportion of the fibers. Furthermore, these properties are also related to the bulk properties of the bonded zones and the spaces or voids in the network represented as a whole by the fiber volume fraction V_f.

This article is aimed at a hybrid structure in which a small volume fraction of synthetic fibers is added to a conventional cellulose pulp. As a result, the existing problems of conventional papers such as low toughness and low failure resistance, which have caused problems in runnability during paper manufacturing, will be alleviated. The use of fiber blends to reinforce material properties has long been a common and successful practice in textile and paper industries. A well known example of the latter is to add pine fibers to standard hardwood pulp to improve paper strength. The analytic investigation using micromechanics on a hybrid fiber network, which we present in this article, has not been reported as far as we are aware. Because of the hybrid nature of the structure, there are some unique problems to be dealt with, such as the hybrid bonding points and their probabilities, and contributions from two different constituent fiber types to system performance. Moreover, compared with previous analyses on paper sheets, the approaches in our article are based on more strict mathematical derivations and are therefore formed into a more systematic theory frame. This in turn enables us to reach some new conclusions about the relationships between the structural characteristics and the mechanical behavior of the fibrous systems.

Nomenclature

A_j: cross-sectional area of the system in direction j

A_{fi}: cross-sectional area of fiber type i

$\bar{b}$, $\bar{b}_f$, and $\bar{b}_b$: mean values of microelement length, free fiber length, and length of bonded portion

C_j: external load in direction j exerted on each bonding point

C_{jp} and C_{jn}: tangential and normal components of C_j

D_i and D: diameter of fiber type i and probabilistic mean diameter of the two fiber types

E_{jj}: system elastic modulus in direction j

E_{fi}, E_{flk}, and E_{fik}: elastic modulus of fiber type i, transverse elastic modulus of the crossing fiber type k, and equivalent tensile modulus of a bonding area with fiber k crossing fiber i

G_{bik}: shear modulus of bonding area between fiber types i and k

I_{fi}: moment of inertia of fiber type i

K_j: geometric coefficient when $\bar{b}$ is projected to direction j

l_i and l: lengths of fiber type i and probabilistic mean length of the two fiber types

M_{jr}' and M_{jr}'': geometric coefficients associated with the two components of deformation caused by T_j in direction r

m_l and n_l: proportional factors between $\bar{b}$, $\bar{b}_f$, and $\bar{b}_b$

n, $\bar{n}$, and $\bar{n}_l$: total number of bonding points in volume V, mean number of bonding points on an arbitrary fiber, and mean number of bonding points per unit length of fiber

P_{ij} and P_i: probabilities of fiber type i bonded with fiber type j and of free fiber segment being fiber type i

t_b and t_{fi}: fiber bond thickness and thickness of the cellulose fiber type i

T_j: total external load in direction j exerted on the system

V_f, V_{f1}, and V_{f2}: fiber volume fractions of the total, fiber type 1, and fiber type 2

V_{fe} and V_{fm}: effective fiber volume fraction due to fiber bonding, and maximum fiber volume fraction without causing multiple fiber overlapping

V_1 and V_2: fiber volume fraction ratios or blend ratios for two fiber types 1 and 2, with $V_1 = V_{f1}/V_f$ and $V_2 = V_{f2}/V_f$

X_1, X_2 and X_3: Cartesian coordinates

θ and ϕ: polar and azimuthal angles

δ, δ_1, δ_2, and δ_3: total deformation, deformations of the free fiber segment due to bending and to elongation, and deformation of the bonded portion, respectively

$\overline{\delta}_{jr}$, $\overline{\delta}_{jr1}$, $\overline{\delta}_{jr2}$, and $\overline{\delta}_{jr3}$: statistical mean deformation components in direction r due to T_j, including total deformation, deformation of free fiber segments due to bending and to elongation, and deformation of bonded portion, respectively

ϵ_{jj} and σ_{jj}: continuum tensile strain and stress of the system in direction j

ν_{jr}: Poisson's ratio of the system

Hybrid Bonding Points and Their Probabilities in a Fibrous Network

Suppose the whole system of this hybrid structure contains two kinds of fibers (a cellulosic as fiber 1 and a synthetic as fiber 2) with corresponding fiber volume fractions V_{f1} and V_{f2}, respectively. The total fiber volume fraction is

$$V_f = \frac{V_{\text{fiber}}}{V_{\text{total}}} = V_{f1} + V_{f2} \quad . \tag{1}$$

The volume fraction ratio of the total fiber volume of fiber type $i = 1$ and 2 in the paper pulp is

$$V_i = \frac{V_{fi}}{V_f} \quad , \tag{2}$$

where

$$V_1 + V_2 = 1 \quad . \tag{3}$$

This is a hybrid fibrous planar network with fibers bonded together during manufacturing through a hydrogen bond mechanism [17].

One way to deal with such a hybrid fibrous structure is to consider the probabilities of different bonding situations between the two fiber types. The bonding points and the free fiber segments between the bonding points as well as their corresponding probabilities consist of the following possible combinations. In the parentheses below, P_{ij} is the probability of fiber type i bonded with fiber type j, and P_i is the probability that the free fiber segment between the two fiber bonds is a fiber of type i, *i.e.*,

(P_{11}): fiber type 1 bonded to fiber type 1, → (P_1) fiber segment type 1.
(P_{12}): fiber type 1 bonded to fiber type 2, → (P_1) fiber segment type 1.
(P_{21}): fiber type 2 bonded to fiber type 1, → (P_2) fiber segment type 2.
(P_{22}): fiber type 2 bonded to fiber type 2, → (P_2) fiber segment type 2.

The values of these probabilities are to be determined.

Characterizing the Microstructural Components of a Hybrid Fibrous System

A general fibrous structure is illustrated in Figure 1. As mentioned earlier, we assume that all the properties of such a system are determined collectively by the bonded areas, the free fiber segments between the bonding points, and the volume ratios of fibers and voids in the structure. Therefore, we have to focus our attention first on the characterization of this microstructure or, more specifically, on an investigation of the density and distribution of the bonding points, the relative proportions of the bonded portion, and the free fiber segment between two bonding points on a fiber in a system of given volume V.

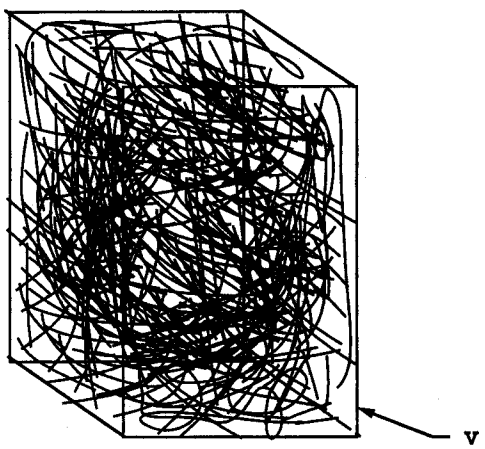

FIGURE 1. A typical fibrous system of volume V.

The approach we use was pioneered by Komori and Makishima [12], who reported on the microstructural

characterization of fibrous assemblies where no bonding exists between fibers and only one fiber type forms the system. Since in our article, we are looking at a bonded hybrid fibrous network consisting of two fiber types that differ in both dimensional and mechanical properties, we have had to modify Komori and Makishima's method. For generality, we have developed the following analyses based on a three-dimensional system; later we show that the result is readily applicable to our planar two-dimensional network.

We first define a Cartesian coordinate system X_1, X_2, X_3 in a fibrous structure. Let the angle between the X_3 axis and the axis of an arbitrary fiber be θ, and that between the X_1 axis and the normal projection of the fiber axis onto the X_1X_2 plane be ϕ. Then the orientation of any fiber can be defined uniquely by a pair (θ, ϕ), provided $0 \leq \theta \leq \pi$ and $0 \leq \phi \leq \pi$, as shown in Figure 2.

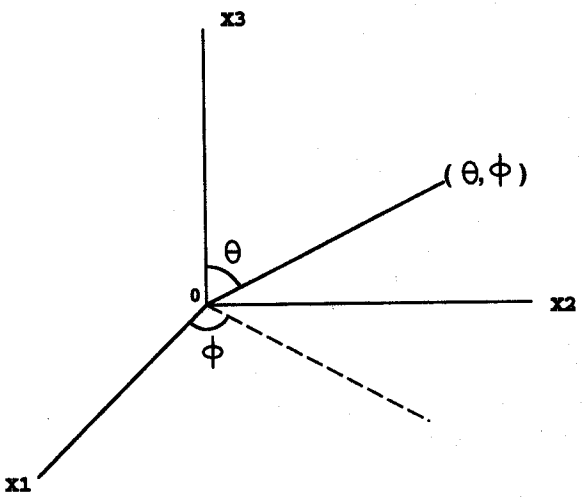

FIGURE 2. System coordinates and fiber orientation.

Let the probability of finding the orientation of a fiber in the infinitesimal range of angles $\theta \sim \theta + d\theta$ and $\phi \sim \phi + d\phi$ be $\Omega(\theta, \phi) \sin \theta d\theta d\phi$, where $\Omega(\theta, \phi)$ is the still unknown density function of fiber orientation, and $\sin \theta$ is the Jacobian of the vector of the direction cosines corresponding to θ and ϕ.

Suppose there are N fibers of straight cylinders of diameter D' and length l' in the fibrous system. According to Komori and Makishima [12], if fiber A of orientation (θ, ϕ) and fiber B of orientation (θ', ϕ') are in contact within the volume V, the two fibers will define a parallelepiped equivalent to that shown in Figure 3. The bases of this parallelepiped are rhombuses whose sides are of length l', and the side planes are perpendicular to the bases and of height $2D'$. The volume v of this parallelepiped is

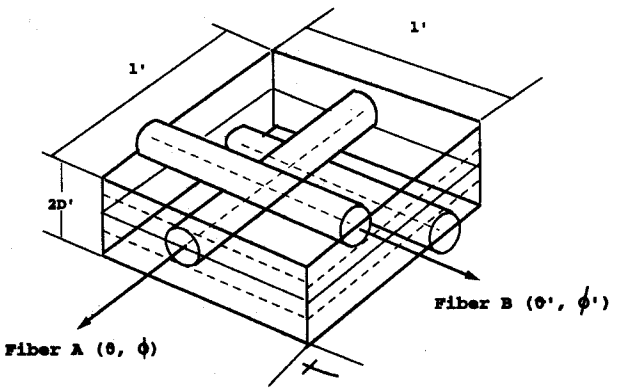

FIGURE 3. Parallelepiped formed by fibers A and B in contact [12].

$$v(\theta, \phi; \theta', \phi') = 2D'l'^2 \sin \chi \quad , \qquad (4)$$

where χ is the angle between the two axes of fibers A (θ, ϕ) and B (θ', ϕ'), and

$$\sin \chi = [1 - (\cos \theta \cos \theta' + \sin \theta \sin \theta' \cos (\phi - \phi'))^2]^{1/2} \quad . \qquad (5)$$

Unfortunately, as Komori and Makishima pointed out, in practice the assumption of straight cylinders is often not the case. Yet others have proved that, for a monocomponent fibrous assembly, the crimp of fibers, the noncylindrical fiber cross section [12], and the length variation of fibers [21] will not affect the validity of this analysis, so long as the mean fiber length and an equivalent mean fiber diameter are used in the equations.

For a hybrid system, however, the dimensional or geometric differences between the two fiber types have to be taken into account, since typically these differences are significant. In our case, the shape of the cross section of the synthetic fiber is reasonably close to a cylinder, whereas the cellulosic fibers have collapsed totally during processing and so possess a flattened cross section. Consequently, the geometries in the preceding analysis have to be modified: the lengths of the sides of the rhombuses may not be the same (should be l_i and l_j), and the height of the side planes should be $D_i + D_j$ instead of $2D'$; here $i, j = 1$ or 2, representing two different fiber types.

Nevertheless, the volume v of this new parallelepiped can still be expressed as

$$v(\theta, \phi; \theta', \phi') = 2Dl^2 \sin \chi \quad , \qquad (6)$$

so long as we bring all the contact probabilities into the equation and define a probabilistic mean diameter as

$$2D = 2D_1P_{11} + (D_1 + D_2)P_{12} + (D_2 + D_1)P_{21} + 2D_2P_{22} \quad (7)$$

or

$$D = D_1P_{11} + (D_1 + D_2)P_{12} + D_2P_{22} \quad , \quad (8)$$

and a probabilistic mean length as

$$l = l_1P_{11} + (l_1 + l_2)P_{12} + l_2P_{22} \quad . \quad (9)$$

By doing so, we have obtained an equation with the same expression as Komori and Makishima's and have meanwhile included the effect of the hybrid components in the analysis. As a result, Komori and Makishima's analysis [12] can be applied here, exactly as if we were dealing with a monocomponent fibrous system, provided D and l are the probabilistic mean values as defined above. So according to reference 12, the mean length $\bar{b}$ between the centers of two neighboring bonding points on the fiber, as illustrated in Figure 4, can be expressed as

$$\bar{b} = \frac{V}{2DLI} \quad , \quad (10)$$

where $L = Nl$ is the total fiber length within volume V, and I represents the overall mean value of sin χ.

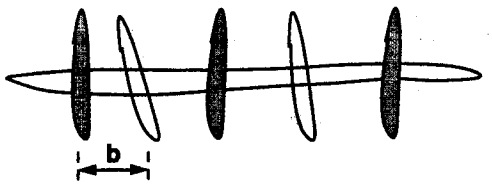

FIGURE 4. A typical fiber in the fiber network and the mean free fiber segment between bonding points.

Furthermore, if we examine a typical structural element of the system in Figure 5, we clearly see that it consists of two bonded portions of mean length $\bar{b}_b$ and one free fiber segment of mean length $\bar{b}_f$. Hence we have

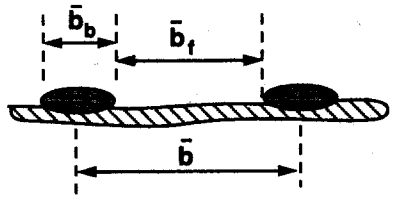

FIGURE 5. A typical microelement and the characteristic dimensions.

$$\bar{b} = \bar{b}_f + \bar{b}_b \quad (11)$$

or

$$\bar{b}_f = \bar{b} - \bar{b}_b = m_l\bar{b} \quad (12)$$

and

$$\bar{b}_b = n_l\bar{b} \quad , \quad (13)$$

where

$$m_l = \frac{\bar{b}_f}{\bar{b}} \quad (14)$$

and

$$m_l + n_l = 1, \quad 0 \le m_l \le 1, \quad \text{and} \quad 0 \le n_l \le 1 \quad (15)$$

are the undetermined coefficients representing the relative proportions of the bonding portion and the free fiber length. Two extreme cases are that when $m_l = 0$ and $n_l = 1$, the fibers are totally bonded together, whereas $m_l = 1$ and $n_l = 0$ represent the case where the bonded area doesn't exist.

Because of the different orientations of the fibers, the lengths of the bonded portions on a fiber vary depending on the directions of all fibers involved. Consequently, we have to use a procedure similar to that for deriving $\bar{b}$ to obtain the statistical mean values $\bar{b}_b$ and $\bar{b}_f$. By examining the views of the bonded portion on a fiber shown in Figure 6, we have for such an arbitrary case

$$b_b = \frac{D}{\sin \chi} \quad , \quad (16)$$

where $0 \le \chi \le \pi$ is the angle formed by two crossing

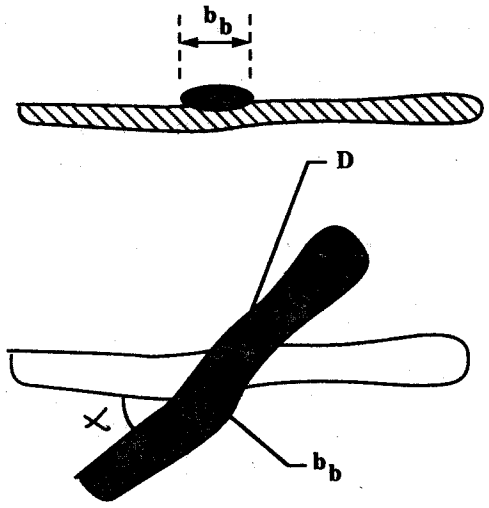

FIGURE 6. Geometry of the bonding portion.

fibers whose expression is given in Equation 5. Note that in Equation 16, when sin χ approaches 0, the value of b_b will become infinite, which is of course impractical. Since in practice the value of b_b ranges from D (fiber diameter) to l (fiber length), the following conditions are used to confine the upper and lower limits of sin χ:

$$\pi - \sin^{-1}\left(\frac{1}{s}\right) > \chi > \sin^{-1}\left(\frac{1}{s}\right) \quad , \qquad (17)$$

where $s = l/D$ is the so-called fiber aspect ratio. This will eliminate the problem, and the mean value $\bar{b}_b$ can then be derived as

$$\bar{b}_b = DR \quad , \qquad (18)$$

where

$$R = \int_0^{\pi} d\theta \int_0^{\pi} d\phi \Omega(\theta, \phi) J'(\theta, \phi) \sin\theta \quad , \qquad (19)$$

and

$$J'(\theta, \phi) = \int_{\theta_1'}^{\theta_2'} d\theta' \int_{\phi_1'}^{\phi_2'} d\phi' \Omega(\theta', \phi') \frac{1}{\sin\chi} \sin\theta' \quad , \qquad (20)$$

where the integral limits θ_1', θ_2', ϕ_1', and ϕ_2' are determined from Equations 17 and 5.

Now we are able to obtain the values of m_l and n_l according to the definitions above, and brining in Equations 10 and 18 gives

$$m_l = \frac{\bar{b} - \bar{b}_b}{\bar{b}} = 1 - \frac{8V_f IR}{\pi} \quad , \qquad (21)$$

where $V_f = \dfrac{\pi D^2 L}{4V}$ is the total fiber volume fraction of the system. The value of n_l follows as

$$n_l = 1 - m_l \quad . \qquad (22)$$

Finally the total bond number n in the volume V containing N fibers, each having $\bar{n}$ bonded points, is [12]

$$n = \frac{N}{2}\bar{n} = \frac{DN^2 l^2}{V} I = \frac{DL^2}{V} I \quad . \qquad (23)$$

The factor $^1/_2$ is introduced to avoid double counting of each bonding point.

Determining the Hybrid Bonding Probabilities

The total number of bond points n in the volume V can also be written as

$$n = \frac{DL^2}{V} I = \frac{D(L_1 + L_2)^2}{V} I \quad , \qquad (24)$$

where

$$L_1 = N_1 l_1, \quad L_2 = N_2 l_2, \quad L_1 + L_2 = L, \quad N_1 + N_2 = N \quad . \qquad (25)$$

L_1, L_2, N_1, and N_2 are the total fiber lengths and fiber numbers within the volume V, and l_1 and l_2 are the single fiber lengths corresponding to two fiber types, respectively, whereas N and L are the total fiber number and the total fiber length.

Let the overall probability of all possible bonding cases be P; obviously

$$P = \sum_{i,j=1}^{2} P_{ij} = 1 = \frac{\dfrac{D(L_1 + L_2)^2}{V} I}{\dfrac{DL^2}{V} I} = \frac{(L_1 + L_2)^2}{L^2} \quad . \qquad (26)$$

Since we have used D (the probabilistic mean diameter) as the diameter for all fibers, the fiber volume fraction ratio can be approximated by

$$V_i = \frac{V_{fi}}{V_f} = \frac{L_i}{L} \text{ or } L_i = V_i L \quad . \qquad (27)$$

Therefore, it follows from Equation 26 that

$$P = \frac{L_1^2 + 2L_1L_2 + L_2^2}{L^2} = \frac{L_1^2}{L^2} + \frac{2L_1L_2}{L^2} + \frac{L_2^2}{L^2} = P_{11} + P_{12} + P_{21} + P_{22} \quad , \qquad (28)$$

where

$$P_{11} = \frac{L_1^2}{L^2} \quad ,$$

$$P_{12} = P_{21} = \frac{L_1 L_2}{L^2} \quad ,$$

$$P_{22} = \frac{L_2^2}{L^2} \quad .$$

Replacing L_1 and L_2 yields

$$P_{11} = \frac{(V_1 L)^2}{L^2} = V_1^2 \quad , \qquad (29)$$

$$P_{12} = P_{21} = \frac{V_1 L V_2 L}{L^2} = V_1 V_2 \quad , \qquad (30)$$

and

$$P_{22} = \frac{(V_2 L)^2}{L^2} = V_2^2 \quad . \qquad (31)$$

The probability P_i of different types of fiber segments between the bonding points is given by

$$P_1 = P_{11} + P_{12} = V_1^2 + V_1V_2 = V_1 \quad (32)$$

and

$$P_2 = P_{21} + P_{22} = V_2^2 + V_1V_2 = V_2 \quad . \quad (33)$$

Some Fundamental Concepts in Treating a Discrete System

Micromechanics is often used to study the mechanical behavior of discrete media from microstructural considerations and is based on the properties of its constituents. However, the inherent random nature of the physical and geometric features of discrete media is fundamentally different from the macroscopic level of the assumed continuum when using the method of combined microanalysis and continuum theory. Therefore, the connections between the formulations from the microstructural analysis and the macroscopic performance have to be established as the premises for the discrete media study. Axelrad [1, 2] has proposed that in formulating the mechanics of a discrete medium, three measuring scales should be used to define such a system. The smallest scale is called a "microelement" of the structure. It is a typical representative element of the microstructure of the system on which all the continuum concepts are applicable, since it is a continuum by definition. Then an intermediate scale, called a "mesodomain," containing a statistical ensemble of the microelements follows. The physical and geometric parameters of the mesodomain are independent of the positions, and have to be derived statistically based on the parameters of its constituent microelements. In fact, the mesodomain is defined as a portion of or as the representative of the whole system on which the continuum approach is once again valid, provided only the effects over distances appreciably greater than the distance between the microelements are concerned [26]. Finally, a finite number of nonintersecting mesodomains form the macroscopic material body. Three such divisions clearly illustrate the relationships between the different structural (from microscopic to macroscopic) levels, and thus actually provide the natural sequence of the micromechanical analysis.

The concepts of these three divisions have been applied, consciously or subconsciously, by previous researchers in dealing with fibrous systems [3, 15, 24]. For the planar fibrous network in this work, it is advantageous to select the typical fiber bonding unit shown in Figure 5 as the microelement. Note that although, as pointed out by Kallmes [8], there are several different bonding states existing in paper systems, the bonding model shown in Figure 5 is by far the dominant form, and so we have adopted it here as the typical microelement. Based on the analysis in the last section, an arbitrary microelement can be represented by a notation $(\bar{b}, \theta, \phi)$. The mesodomain of the macroscopic network is illustrated in Figure 7. The length $\bar{b}_j$ of the mesodomain will be given later.

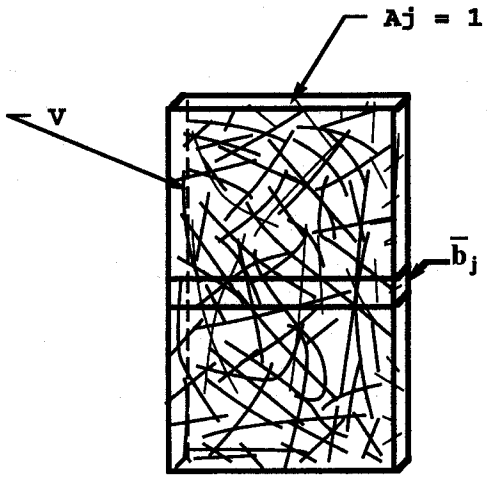

FIGURE 7. A mesodomain of the system.

As stated above, our analysis will first focus on a microelement using continuum approaches. The results will then be statistically extended to the mesodomain level. The overall behavior of the system is eventually derived by applying mesodomain results to the macroscopic medium.

There is another issue about the homogeneity assumption of the fibrous systems. When we apply the well documented continuum elasticity theory to the system, we actually presume the homogeneity, a premise for application of the theory. In reality, fibrous systems essentially consist of two different phases—the fiber mass and the voids between the fibers. Perkins [24] made a brilliant comment in this regard. He claimed, "The property of heterogeneity depends on the level at which one focuses attention and the object of the analysis at hand. For example, all materials could be considered heterogeneous at a molecular level. A good deal of the time, however, one is concerned with some average response of the material which involves such large aggregates of molecules that it is not only expedient but completely justifiable to treat the medium as a homogeneous one." As expressed above, we will apply continuum theory to both the microelement and the macroscopic medium successively. In either case, the magnitude of the dimensional scale we focus on is

far greater than the voids within the internal structure of the objects, and the objects therefore can be reasonably treated as homogeneous media.

Components of the External Loads Acting on a Bonding Point

Suppose, as shown in Figure 8A, that there is an external tensile load T_j being exerted on a fiber network in direction j ($j = 1$ *or* 2). This load has to be transmitted through each bonding point and sustained by all these bonding points. Since the orientations of fibers and their bonding areas are very different, it is difficult to determine the actual direction and magnitude of the force C acting on each bonding point. However, if we cut a cross section of the network and denote all the components in direction j of the forces acting on the bonding points as C_j, we can see clearly that the resultant force formed by the components C_j balances the external load T_j (Figure 8B). Because of the isotropy of the system, it is reasonable to assume that all these C_j have the identical magnitude, which can thus be obtained directly as

$$C_j = \frac{T_j}{n_{\bar{b}_j}} \quad , \tag{34}$$

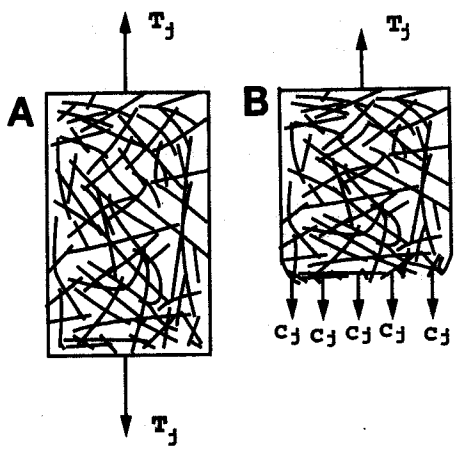

FIGURE 8. External load and load equilibrium: (A) load T_j applied to the system at direction j, and (B) load equilibrium.

where $n_{\bar{b}_j}$ is the total number of bonding points involved and is to be determined. Moreover, Lee [15] proved that for a bonding point on an arbitrary fiber (θ, ϕ), the force C_j acting on this point can be resolved into the tangential component C_{jp} along the axis of the fiber and the normal component C_{jn} perpendicular to the fiber axis, as shown in Figure 9. These components for a planar case can be expressed as [15]

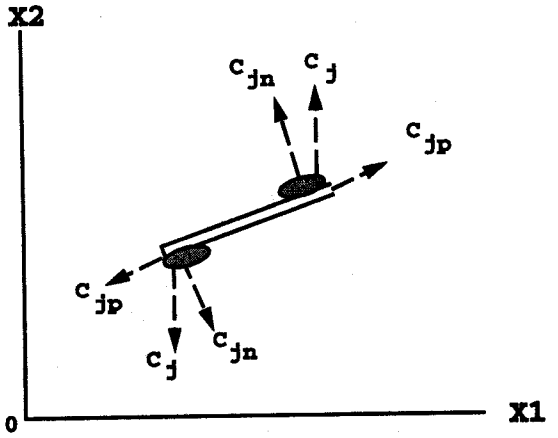

FIGURE 9. Force resolution at bonding points.

$$C_{1p} = C_1 \sin\theta \cos\phi(\sin\theta \cos\phi i_1 + \sin\theta \sin\phi i_2) \quad , \tag{35}$$

$$C_{2p} = C_2 \sin\theta \sin\phi(\sin\theta \cos\phi i_1 + \sin\theta \sin\phi i_2) \quad , \tag{36}$$

$$C_{1n} = C_1[(1 - \sin^2\theta \cos^2\phi)i_1 - (\sin^2\theta \sin\phi \cos\phi)i_2] \quad , \tag{37}$$

$$C_{2n} = C_2[-\sin^2\theta \sin\phi \cos\phi i_1 + (1 - \sin^2\theta \sin^2\phi)i_2] \quad . \tag{38}$$

These equations provide us with the relationships between the orientation of an arbitrary fiber and the forces acting on it.

Deformation of a Typical Microelement Under Uniaxial Tensile Loading

In order to continue the derivation, we have to make the following assumptions:

1. All the constituent fibers of the same type have identical properties with the fiber axis of symmetry, are uniform along their length, and are linearly elastic unless specified otherwise.
2. Each fiber segment of the microelement is straight before loading. This assumption is necessary, as shown below, so that the analysis of fiber segment deformation will be tractable.
3. Torsional and compressional deformation of the fiber segments is so small that it is neglected.
4. For simplicity, we focus on the paper structure before pressing, excluding the severe structural distortion due to high pressure pressing by the machine.

Let us now examine a typical microelement $(\bar{b}, \theta,$

ϕ) taken from the system (Figure 9). As specified before, this microelement consists of two bonding points with a free fiber segment of length $\bar{b}_f$ between them. On each bonding point, there are the normal and tangential components C_{jn} and C_{jp} ($j = 1, 2$) due to the external loading. The normal components C_{jn} acting on the two neighboring bonding points form a torque couple that will bend the fiber segment, whereas the tangential components C_{jp} acting on the two bonding points will stretch both the bonding portion and the fiber segment along the fiber axis, as illustrated in Figure 9. The overall deformation $\delta = \delta(\theta, \phi)$ of the microelement therefore consists of three parts, similar to that suggested by Perkins [24]:

$$\delta = \delta_{\text{bend}} + \delta_{\text{axial}} + \delta_{\text{bonded}} = \delta_1 + \delta_2 + \delta_3 \quad , \quad (39)$$

where δ_{bend} represents the bending deformation of the fiber segment, δ_{axial} is the tensile elongation of the fiber segment, and δ_{bonded} is the deformation of the bonded portion.

First of all, considering the structure of the microelement in which the fiber segment can be treated as a beam with built-in ends, the bending deflection of the type i fiber segment can be readily derived as

$$\delta_{\text{bend}}{}^{i} = \frac{C_{jn}(\bar{b}_f)^3}{3E_{fi}I_{fi}} = \frac{C_{jn}(m_i\bar{b})^3}{3E_{fi}I_{fi}} \quad . \quad (40)$$

The elongation of the type i fiber segment due to C_{jp} is

$$\delta_{\text{axial}}{}^{i} = \frac{C_{jp}m_i\bar{b}}{A_{fi}E_{fi}} \quad , \quad (41)$$

where A_{fi}, I_{fi}, and E_{fi} are the cross-sectional area, the moment of inertia, and the elastic modulus of fiber type i, respectively.

We can obtain the deformation of the bonded portions δ_{bonded} from Perkins' analysis [24], where the bonded portion of a microelement with fiber type i as the fiber segment and type k as the crossing fiber was modeled as a shear lag problem of a strip (the lower fiber) subjected to an applied load, say, C_{jp}:

$$\delta_{\text{bonded}}{}^{ik} = \frac{C_{jp}n_i\bar{b}\left(\frac{E_{fi}}{E_{fik}} + \frac{\tanh K}{K}\right)}{2E_{fi}A_{fi}\left(1 + \frac{E_{fi}}{E_{fik}}\right)} \quad , \quad (42)$$

where $K = \dfrac{K_b n_i \bar{b}}{2}$ and

$$K_b = \sqrt{\frac{G_{bik}}{t_b t_f}\frac{(E_{fi} + E_{fik})}{E_{fi}E_{fik}}} \quad . \quad (43)$$

Here, G_{bik} represents the bonding material shear modulus between fiber type i and k, t_b is the bond thickness, t_{fi} is the thickness of fiber type i, and E_{fik} is the transverse elastic modulus of the crossing fiber k.

If we designate an equivalent tensile modulus for the bonded portion as

$$E_{fik} = \frac{2E_{fi}\left(1 + \frac{E_{fi}}{E_{fik}}\right)}{\left(\frac{E_{fi}}{E_{fik}} + \frac{\tanh K}{K}\right)} \quad , \quad (44)$$

$\delta_{\text{bonded}}{}^{ik}$ can then be expressed in a more concise form:

$$\delta_{\text{bonded}}{}^{ik} = \frac{C_{jp}n_i\bar{b}}{A_{fi}E_{fik}} \quad . \quad (45)$$

In addition, since we have two fiber types and hence various bonding situations with different fiber segments, each having its own probability, the overall deformation of such an arbitrary microelement should be fully expressed as

$$\delta = \delta_1 + \delta_2 + \delta_3 = \sum_{i=1}^{2} [\delta_{\text{bend}}{}^{i}]P_i + \sum_{i=1}^{2} [\delta_{\text{axial}}{}^{i}]P_i + \sum_{i,k=1}^{2} [\delta_{\text{bonded}}{}^{ik}]P_{ik} \quad . \quad (46)$$

Mesodomain Deformation from the Microelement Analysis

The mesodomain shown in Figure 7 is by definition a portion of the network and consists of a statistical ensemble of microelements. The key issue in extending the analysis on a microelement to this mesodomain is to obtain the geometric and deformational relations between the two structural levels. Note that all the microelements with mean length $\bar{b}$ in this mesodomain are distributed with various orientations.

Based on the analysis developed by Lee and Lee [14], the mean values of the length projections of the microelements ($\bar{b}$, θ, ϕ) on the two planar directions $\bar{b}_j$ ($j = 1, 2$), as shown in Figure 10, can be derived as

$$\bar{b}_j = \bar{b}K_j = \frac{V}{2DLI}K_j \quad , \quad (47)$$

where

$$K_1 = \int_0^{\pi} d\theta \int_0^{\pi} d\phi \sin^2\theta \cos\phi\Omega(\theta, \phi) \quad (48)$$

and

$$K_2 = \int_0^{\pi} d\theta \int_0^{\pi} d\phi \sin^2\theta \sin\phi\Omega(\theta, \phi) \quad . \quad (49)$$

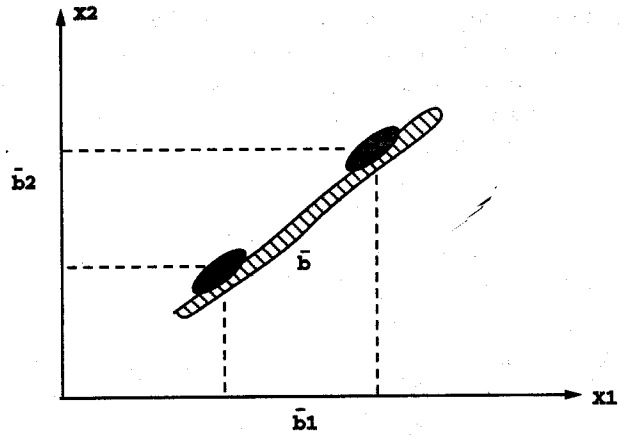

FIGURE 10. Projections of a microelement.

Unlike the case of a continuum, where we can readily define the stress on a structural unit by dividing the external load by the area it is being exerted on, for this discrete system we have to deal with the individual contact points instead of the area, since they are the basic structural units and the only mechanism to transfer and sustain the load. Note also that the number of bond points in the system depends on the volume concerned. Therefore, it is necessary to designate a mesodomain that has a well defined volume or length for a given cross-sectional area, so that the contact points in it will be a constant. Considering the physical meaning of $\bar{b}_j$, it is desirable that $\bar{b}_j$ be selected as the length of the mesodomain, as seen in Figure 7.

Assume without losing generality that this mesodomain is taken from a macroscopic system of volume V with a unit area of cross section, and its length is $\bar{b}_j$. The volume of the mesodomain will then be $\Delta V = \bar{b}_j$. The number of bonding points in this mesodomain can be calculated [14] proportionally as

$$n_{\bar{b}_j} = n\frac{\bar{b}_j}{V} = \frac{L}{2V}K_j \quad . \tag{50}$$

Therefore, from Equation 34 in the previous section, the magnitude of the force on each bonding point within this mesodomain can now be calculated as

$$C_j = \frac{T_j}{n_{\bar{b}_j}} = \frac{2VT_j}{LK_j} \quad . \tag{51}$$

The mechanical deformation of this mesodomain results from the deformation of all the microelements in it. Since the orientations of the microelements and the acting forces are different and distributed according to the fiber orientation density function, the statistical mean values have to be used. The statistical mean $\bar{\delta}_{jr}$ of the deformation of all microelements within the mesodomain in direction r due to the external load T_j can be derived according to Lee and Lee [14] by integrating Equation 46, the overall deformation of a typical microelement, over all possible ranges of distribution using the density function, *i.e.*,

$$\bar{\delta}_{jr} = \int_0^{\pi} d\theta \int_0^{\pi} d\phi\,\delta\Omega(\theta,\phi)$$

$$= [+\bar{\delta}_1 M_{jr}' \pm \bar{\delta}_2 M_{jr}'' \pm \bar{\delta}_3 M_{jr}'''] \qquad (\pm : +j = r, -j \neq r) \quad , \tag{52}$$

where (from Equations 40 and 46)

$$\bar{\delta}_1 = \sum_{i=1}^{2} \frac{C_j(m_i\bar{b})^3}{3E_{fi}I_{fi}} P_i \quad , \tag{53}$$

(from Equations 41 and 46)

$$\bar{\delta}_2 = \sum_{i=1}^{2} \frac{C_j m_i \bar{b}}{A_{fi}E_{fi}} P_i \quad , \tag{54}$$

and (from Equations 45 and 46)

$$\bar{\delta}_3 = \sum_{i,k=1}^{2} \frac{C_j n_i \bar{b}}{A_{fi}E_{fik}} P_{ik} \tag{55}$$

are the magnitudes corresponding to the three different forms of microelement deformation, and M_{jr}' and M_{jr}'' are the respective coefficients representing the effects of fiber and load orientation. M_{jr}' can be expressed [3] as

$$M_{11}' = \int_0^{\pi} d\theta \int_0^{\pi} d\phi(1 - \sin^2\theta\cos^2\theta)\Omega(\theta,\phi)\sin\theta \quad , \tag{56}$$

$$M_{22}' = \int_0^{\pi} d\theta \int_0^{\pi} d\phi(1 - \sin^2\theta\sin^2\phi)\Omega(\theta,\phi)\sin\theta \quad , \tag{57}$$

$$M_{12}' = M_{21}' = \int_0^{\pi} d\theta \int_0^{\pi} d\phi \sin^3\theta\cos\phi\Omega(\theta,\phi) \quad , \tag{58}$$

and M_{jr}'' can be derived as

$$M_{11}'' = \int_0^{\pi} d\theta \int_0^{\pi} d\phi \sin^3\theta\cos^2\phi\Omega(\theta,\phi) \quad , \tag{59}$$

$$M_{22}'' = \int_0^{\pi} d\theta \int_0^{\pi} d\phi \sin^3\theta\sin^2\phi\Omega(\theta,\phi) \quad , \tag{60}$$

and

$$M_{12}'' = M_{21}'' = M_{12}' = M_{21}' \quad . \tag{61}$$

The expressions of the deformation components can be rearranged as

$$\bar{\delta}_1 = \frac{C_j}{3A_1}(m_i\bar{b})^3 \quad , \tag{62}$$

$$\bar{\delta}_2 = \frac{C_j}{A_2}(m_i\bar{b}) \quad , \tag{63}$$

and

$$\bar{\delta}_3 = \frac{C_j}{A_3}(n_i\bar{b}) \quad , \tag{64}$$

where

$$A_1 = \frac{1}{\left(\frac{P_1}{E_{f1}I_{f1}} + \frac{P_2}{E_{f2}I_{f2}}\right)} \quad , \tag{65}$$

$$A_2 = \frac{1}{\left(\frac{P_1}{E_{f1}A_{f1}} + \frac{P_2}{E_{f2}A_{f2}}\right)} \quad , \tag{66}$$

and

$$A_3 = \frac{1}{\left(\frac{P_{11}}{E_{f11}A_{f1}} + \frac{P_{12}}{E_{f12}A_{f1}} + \frac{P_{21}}{E_{f21}A_{f2}} + \frac{P_{22}}{E_{f22}A_{f2}}\right)} \quad . \tag{67}$$

Elastic Moduli and Poisson's Ratios of the System

The value $\bar{\delta}_{jr}$ shown above is the statistical mean deformation of all microelements within that mesodomain $\Delta V = \bar{b}_j$. It is actually the overall deformation of the mesodomain itself of length $\bar{b}_j$ in the direction r due to the external load T_j. Since the mesodomain is part of the system, we may thus define the continuum strain of the system as

$$\epsilon_{jj} = \frac{\bar{\delta}_{jj}}{\bar{b}_j} \tag{68}$$

and the continuum stress as

$$\sigma_{jj} = \frac{T_j}{A_j} \quad , \tag{69}$$

where A_j is the area of the loading cross section of the system. In this case, we have $A_j = 1$. Furthermore, we may define the elastic moduli of the system as

$$E_{jj} = \frac{\sigma_{jj}}{\epsilon_{jj}} = \frac{T_j\bar{b}_j}{[\bar{\delta}_1 M_{jj}' + \bar{\delta}_2 M_{jj}'' + \bar{\delta}_3 M_{jj}'']} \quad (j = 1, 2) \tag{70}$$

and the Poisson's ratios as

$$\nu_{jr} = -\frac{\frac{\bar{\delta}_{jr}}{\bar{b}_r}}{\frac{\bar{\delta}_{jj}}{\bar{b}_j}} = \frac{\epsilon_{jr}}{\epsilon_{jj}} \quad (j \neq r \text{ and } j, r = 1, 2) \quad . \tag{71}$$

More specifically, we can decompose the overall modulus into three parts representing the contributions from both the free fiber segments and the bonded portions of the microelements:

$$E_{jj}' = \frac{T_j\bar{b}_j}{\bar{\delta}_1 M_{jj}'}, \; E_{jj}'' = \frac{T_j\bar{b}_j}{\bar{\delta}_2 M_{jj}''}, \; E_{jj}''' = \frac{T_j\bar{b}_j}{\bar{\delta}_3 M_{jj}''} \quad . \tag{72}$$

Equation 70 may then be rewritten as

$$\frac{1}{E_{jj}} = \frac{1}{E_{jj}'} + \frac{1}{E_{jj}''} + \frac{1}{E_{jj}'''} \quad . \tag{73}$$

This form suggests that the whole system may be treated as a series system of three elastic elements with moduli E_{jj}', E_{jj}'', and E_{jj}''', respectively, as commonly depicted in Figure 11.

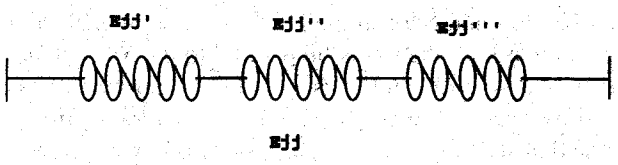

FIGURE 11. Analogy of the system modulus and its components.

Furthermore the Poisson's ratios of the system can be derived as

$$\nu_{jr} = -\frac{\frac{\bar{\delta}_{jr}}{\bar{b}_r}}{\frac{\bar{\delta}_{jj}}{\bar{b}_j}} = -\frac{\bar{\delta}_{jr}\bar{b}_j}{\bar{\delta}_{jj}\bar{b}_r} = \frac{[\bar{\delta}_1 M_{jr}' + \bar{\delta}_2 M_{jr}'' + \bar{\delta}_3 M_{jr}'']\bar{b}_j}{[\bar{\delta}_1 M_{jj}' + \bar{\delta}_2 M_{jj}'' + \bar{\delta}_3 M_{jj}'']\bar{b}_r} \; (j \neq k) \quad . \tag{74}$$

Thus, the Poisson's ratios can be divided into three portions as well:

$$\nu_{jr} = \nu_{jr}' + \nu_{jr}'' + \nu_{jr}'''$$

$$= \frac{\bar{\delta}_1 M_{jr}' \bar{b}_j}{[\bar{\delta}_1 M_{jj}' + \bar{\delta}_2 M_{jj}'' + \bar{\delta}_3 M_{jj}'']\bar{b}_r} + \frac{\bar{\delta}_2 M_{jr}'' \bar{b}_j}{[\bar{\delta}_1 M_{jj}' + \bar{\delta}_2 M_{jj}'' + \bar{\delta}_3 M_{jj}'']\bar{b}_r} + \frac{\bar{\delta}_3 M_{jr}'' \bar{b}_j}{[\bar{\delta}_1 M_{jj}' + \bar{\delta}_2 M_{jj}'' + \bar{\delta}_3 M_{jj}'']\bar{b}_r} \quad , \quad (75)$$

where

$$\nu_{jr}' = \frac{\bar{\delta}_1 M_{jr}' \bar{b}_j}{[\bar{\delta}_1 M_{jj}' + \bar{\delta}_2 M_{jj}'' + \bar{\delta}_3 M_{jj}'']\bar{b}_r} \quad , \quad (76)$$

$$\nu_{jr}'' = \frac{\bar{\delta}_2 M_{jr}'' \bar{b}_j}{[\bar{\delta}_1 M_{jj}' + \bar{\delta}_2 M_{jj}'' + \bar{\delta}_3 M_{jj}'']\bar{b}_r} \quad , \quad (77)$$

and

$$\nu_{jr}''' = \frac{\bar{\delta}_3 M_{jr}'' \bar{b}_j}{[\bar{\delta}_1 M_{jj}' + \bar{\delta}_2 M_{jj}'' + \bar{\delta}_3 M_{jj}'']\bar{b}_r} \quad (78)$$

are the components corresponding to the bending deformation of the fiber segments, the contribution of fiber elongation, and the deformation of the bonded area, respectively.

Results for an Isotropic Planar System and the Effect of Fiber Size

In the case of an isotropic planar fibrous network with a random fiber distribution, there are different ways of determining the form of the density function of fiber orientation. We have adopted the one proposed by Komori and Makishima [12]. We assume that for a planar case, all the fibers lie parallel to the X_1X_2 plane, that is $\theta = \pi/2$, and ϕ is randomly distributed uniformly over the range $[0, \pi]$ due to structural isotropy. The density function Ω in this case was derived in reference 12 using Dirac's delta function Δ as

$$\Omega(\theta, \phi) = \frac{1}{\pi} \Delta\left(\theta - \frac{\pi}{2}\right) \quad . \quad (79)$$

With this density function, it is quite straightforward to calculate most of the geometric parameters, such as $K_1 = K_2 = 2/\pi$, $M_{11}' = M_{22}' = M_{11}'' = M_{22}'' = 1/2$, $M_{12}' = M_{21}' = M_{12}'' = M_{21}'' = 1/2\pi$, $I = 2/\pi$.

If we substitute all the expressions for T_j, $\bar{b}_j$, and $\bar{\delta}_{jj}$ $(j = 1, 2)$ along with the calculated values above into Equation 72, we eventually get

$$E_{jj}' = \frac{3}{4}\left(\frac{4}{\pi}\right)^7 \left(\frac{V_f}{m_l}\right)^3 \frac{A_1}{D^4},$$

$$E_{jj}'' = \frac{1}{4}\left(\frac{4}{\pi}\right)^3 \left(\frac{V_f}{m_l}\right) \frac{A_2}{D^2}, \; E_{jj}''' = \frac{1}{\pi R D^2} A_3 \quad , \quad (80)$$

where A_1, A_2, and A_3 are still the same as in Equations 65–67. Similarly, we can obtain from Equation 75 the overall Poisson's ratio,

$$\nu_{jr} = \nu_{12} = \nu_{21} = \frac{1}{\pi} \quad , \quad (81)$$

a constant independent of fiber properties. Its components become

$$\nu_{jr}' = \frac{1}{\pi} \frac{\bar{\delta}_1}{[\bar{\delta}_1 + \bar{\delta}_2 + \bar{\delta}_3]} \quad ,$$

$$\nu_{jr}'' = \frac{1}{\pi} \frac{\bar{\delta}_2}{[\bar{\delta}_1 + \bar{\delta}_2 + \bar{\delta}_3]} \quad ,$$

$$\nu_{jr}''' = \frac{1}{\pi} \frac{\bar{\delta}_3}{[\bar{\delta}_1 + \bar{\delta}_2 + \bar{\delta}_3]} \quad . \quad (82)$$

As for the calculations for m_l and n_l, by taking $I = 2/\pi$ into Equation 21, we get

$$m_l = \frac{\pi^2 - 16 V_f R}{\pi^2} \quad , \quad (83)$$

where R was defined before as the ratio of mean bond length and the fiber diameter. Substituting the form of the density function for a randomly distributed planar system into Equations 18–20 gives

$$R = \frac{1}{\pi^2} \int_0^{\pi} d\phi' \int_{\phi_1}^{\phi_2} d\phi \frac{1}{\sin(\phi - \phi')} \quad , \quad (84)$$

where

$$\phi_1 = \phi' + \sin^{-1}\left(\frac{1}{s}\right), \phi_2 = \pi + \phi' - \sin^{-1}\left(\frac{1}{s}\right) \quad . \quad (85)$$

Eventually, the explicit expression for R can be calculated using Equations 84 and 85:

$$R = \frac{1}{\pi} \ln \cot^2 \frac{\arcsin\left(\frac{1}{s}\right)}{2} \quad . \quad (86)$$

Although this equation shows that the relationship between fiber aspect ratio s and the bonding ratio R is in a rather complex form, R actually decreases monotonically as $1/s$ increases, so far as the principal value of the inverse sine function is concerned, because practically the ratio $1/s = D/l$ ranges in a limited scope.

One way to test this equation is to try some special values. That is, when $D = 0$ or $s \to \infty$, R should approach infinity, as implied in Equation 18. This is true in Equation 86. Also, when $1/s = 1$ or $l = D$, $R = 0$ according to Equation 86, meaning that in the case

where fiber length is equal to its diameter, the bond length will diminish to zero.

If we compute the first derivative of R with respect to $1/s$, we will have

$$\frac{dR}{d\left(\frac{1}{s}\right)} = -\frac{1}{\pi} \frac{1}{\cos^2 \frac{\arcsin\left(\frac{1}{s}\right)}{2} \sqrt{1-\left(\frac{1}{s}\right)^2}} \quad . \quad (87)$$

Note that $s = 1$ is actually a singular point, and therefore should be excluded in our discussion. Its practical meaning is obvious, *i.e.*, a fiber's diameter cannot be greater than its length. Furthermore, as shown in this relation, there is no real solution for equation $dR/d(1/s) = 0$, indicating that there will be no extreme values for R at a given fiber orientation function as we change the fiber dimensions D and l, and confirming the monotonic relation between R and s. Keep in mind that for our hybrid case, the probabilistic mean values D and l of the two fibers will be used here to calculate the value of R.

In the equations above, we calculate the probability terms P_i and P_{ik} from Equations 29 to 33, using the given fiber volume fraction ratios V_i so as to provide values for A_1, A_2, and A_3 in Equations 65–67. Substituting the results along with given fiber properties such as E_{fi}, I_{fi}, A_{fi}, E_{fik}, and V_f provided in Table I into the corresponding equations will produce the numerical solutions of the system properties.

TABLE I. Fiber properties.

Item	Fiber 1 (cellulose)	Fiber 2 (synthetic)
Young's modulus, GPa	$E_{f1} = 4.1$	E_{f2}
Transverse elastic modulus, GPa[a]	$E_{f11} = 0.32$	$E_{f12} = 0.28$
Shear modulus of bonding area[b]	$G_{b12} = 0.11$	$G_{b21} = 0.11$
Between fiber 1 and 2, GPa		
Between fiber 1 and 1, 2 and 2, GPa	$G_{b11} = 0.11$	$G_{b22} = 0.11$
Mean fiber length, mm	$l_1 = 1.0$	l_2
Mean fiber diameter, mm	$D_1 = t_{f1} = 0.017$	D_2
Mean fiber thickness, mm	$t_{f1} = 0.017$	$t_{f2} = D_2$
Mean fiber width, mm	$w_{f1} = 0.034$	$w_{f2} = D_2$
Fiber moment of inertia	$I_{f1} = \frac{w_{f1}t_{f1}^3}{12}$	$I_{f2} = \eta\frac{\pi D_2^4}{64}$
Fiber cross-sectional area	$A_{f1} = w_{f1}t_{f1}$	$A_{f2} = \frac{\pi D_2^2}{4}$

[a] Estimated based on references 7 and 8. [b] Assumed.

In Equation 80, there is a term V_f/m_l, which, as proven below, is an important structural parameter for a fibrous system. Substituting Equation 21 for m_l into the term gives

$$\frac{V_f}{m_l} = \frac{\pi V_f}{\pi - 8IRV_f} = V_{fe} \quad , \quad (88)$$

where V_{fe} can be considered as the effective fiber volume fraction by taking the effect of fiber bonding into account. If fiber bonding is neglected, we have $R \to 0$ and $m_l \to 1$, so that the equation above reduces to $V_f = V_{fe}$. In other words, the equation implies that the effect of fiber volume fraction has been increased by a factor,

$$\frac{\pi}{\pi - 8IRV_f} > 1 \quad , \quad (89)$$

due to fiber bonding, so that the system becomes stiffer as though there were more fibers. Furthermore, in order to insure a meaningful effective fiber volume fraction *i.e.*, $V_{fe} \geq 0$, there must be from Equation 88

$$\pi > 8IRV_f \quad \text{or} \quad IRV_f < \left(\frac{\pi}{8}\right) \quad . \quad (90)$$

This is the fundamental relationship between the fiber bond parameter R, which is determined by fiber diameter and length at a given fiber orientation function, the fiber orientation indicator I as defined in reference 12, and the fiber volume fraction V_f of the fibrous system. More specifically, as seen in Equation 88, insuring that V_{fe} is meaningful is equivalent to insuring that $m_l \geq 0$ (therefore inequality 89 can also be derived from Equation 21 by setting $m_l \geq 0$), which means that when inequality 90 is violated, the free fiber length between bonds will no longer exist. The excessive fibers will then overlap with each other to create a distorted structure characterized by multilayers, so that the system will no longer be two-dimensional. Therefore, this inequality indicates that for any fibrous system, there is a maximum value of the fiber volume fraction V_{fm} that can be achieved without distorting the system or, in other words, without causing the multiple fiber overlapping. From inequality 90,

$$V_{fm} < \left(\frac{\pi}{8RI}\right) \quad . \quad (91)$$

Calculations and Discussion

There are two different fiber types in our system. Comparing the shapes of both cellulosic and synthetic fibers in the system shows that the latter is closer to the ideal cylinder assumption, but the cellulosic fibers possess a flat shape. The parameters of fiber properties are listed in Table I. The bond thickness $t_b = 0.27$ μm is

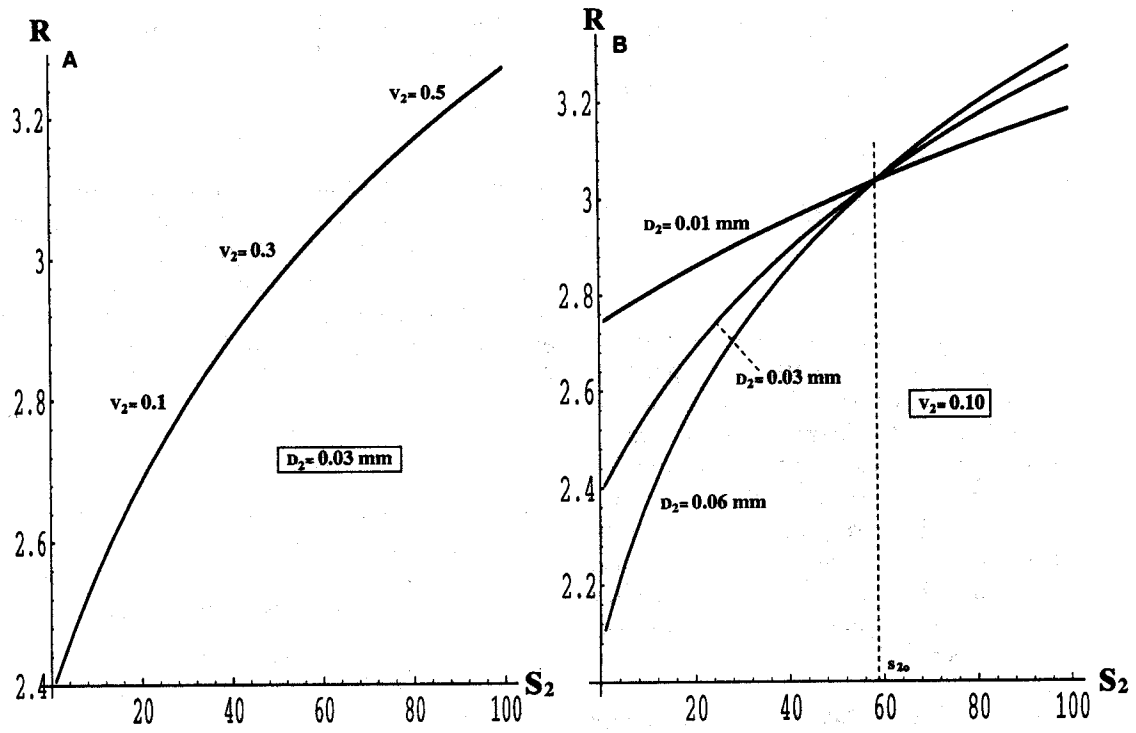

FIGURE 12. Predicted relationship between R value and fiber type 2 properties: (A) R versus the fiber aspect ratio s_2 at three levels of fiber volume fraction ratio V_2, and (B) R versus the fiber aspect ratio s_2 at three levels of fiber diameter D_2.

used in Equation 43 for calculation. In Table I, some key properties of fiber 2 are kept as variables so as to examine their effects on the system properties to be predicted.

Using all the relevant equations above and the fiber properties provided in Table I, we can calculate some of the important microstructural parameters and predict the system moduli and system Poisson's ratio as well as their components. The results of a parametric study of the effects of adding fiber 2 into the system are illustrated in Figures 12–17.

We must point out that, based on the assumptions and the preceding analysis, the system in this study is highly idealized because machine pressing effects during the paper manufacturing process are excluded. Machine pressing at high pressure will compact a paper structure; consequently, the fiber volume fraction value V_f of a real paper will be higher than the values we are going to use in our calculation. Nevertheless, the relationships between the system and fiber properties, the system structure-property correspondences, and other interconnections revealed and predicted in this study, which may only be possible for such an ideal case, should still be useful in understanding the structure and its mechanical behavior of a fibrous network.

CHARACTERISTICS OF STRUCTURAL PARAMETERS

For a bonded fibrous network, two structural parameters are fundamental in describing the system microstructure: first, the ratio of the mean free fiber length and the mean length of the microelement, $m_l = \bar{b}_f/\bar{b}$, indicating the relative proportion of the free fiber length to the total microelement length, and second, the ratio of the mean bond length to the mean fiber diameter, $R = \bar{b}_b/D$, representing the bond size relative to fiber thickness. In our isotropic case, the two parameters are expressed in Equations 83 and 86. Figures 12 and 13 are thus constructed to show how these two parameters are affected by adding the synthetic fiber 2 into the system. Because we need to know the R value before calculating m_l from Equation 83, we will discuss the parameter R first.

As we add fiber 2 into the system, Figure 12A shows that when the diameter of fiber 2 is given, a longer fiber 2 (with a higher aspect ratio s_2) will result in a slightly higher R value, or a greater mean bond length relative to the mean fiber diameter. Moreover, this relation is unaffected by the relative quantity ratio V_2, since the curves corresponding to three different V_2 values coincide with each other. Conversely, when the fiber aspect ratio s_2 is fixed, the relation between the fiber di-

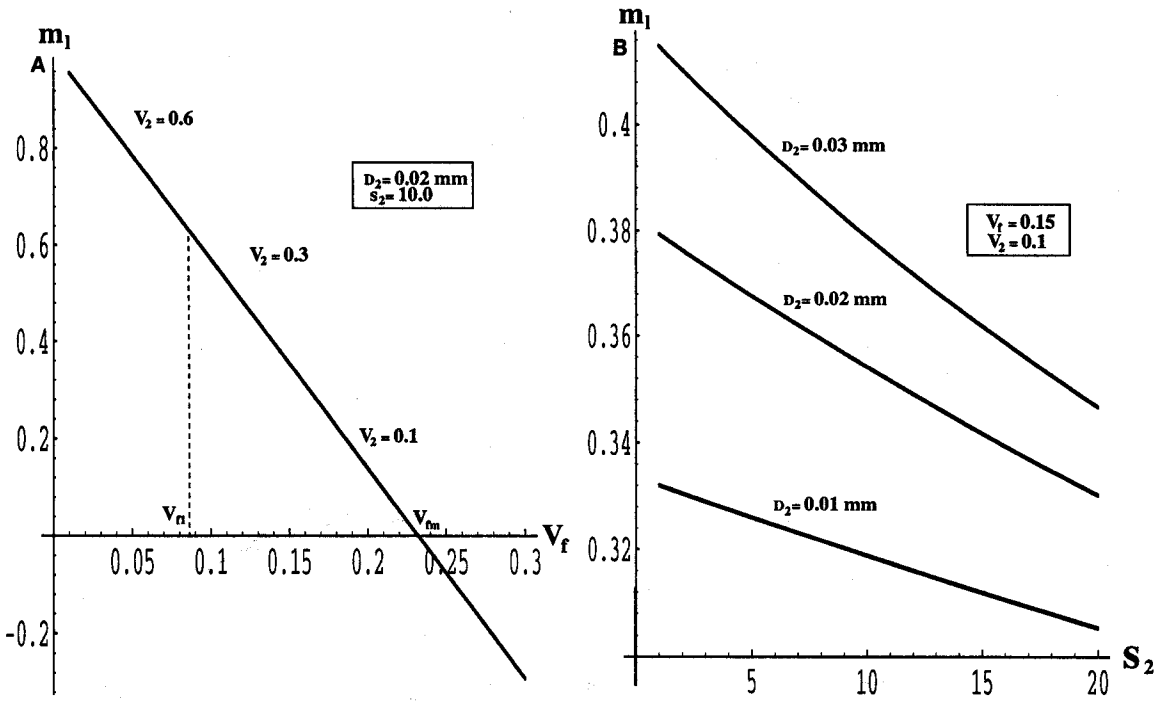

FIGURE 13. Predicted relationship between m_l value and fiber type 2 properties: (A) m_l versus the fiber volume fraction V_f at three levels of fiber volume fraction ratio V_2, (B) m_l versus the fiber aspect ratio s_2 at three levels of fiber diameter D_2.

ameter D_2 and R is not as straightforward. There is a critical level s_{2o}, as indicated by the dotted line on Figure 12B. When $s_2 < s_{2o}$, a thicker fiber 2 will cause a smaller R value, and this trend will reverse when $s_2 > s_{2o}$. R becomes independent of the s_2 value at the point $s_2 = s_{2o}$.

Figure 13a illustrates two facts: First, it tells how a greater total fiber amount will, as expected, cause a decay in the free fiber length, revealed by a decreasing m_l value when we increase the total fiber volume fraction V_f. Since the value m_l cannot be negative, this defines a maximum value V_{fm}, whose expression is shown in inequality 91, allowable in the system in order to avoid structure distortion or multiple layers of fibers so as to maintain a two-dimensional structure. The second fact Figure 13A implies is that the amount of synthetic fiber 2 that can be added into the system formed by fiber 1 alone must be restricted. For instance, if the original system with the cellulose fiber 1 has the total fiber volume fraction V_{f1}, then the maximum quantity of fiber 2 allowable in the system is $V_{f2} = V_{fm} - V_{f1}$. The fiber fraction ratio V_2 has no net effect on m_l when other parameters are given. The size of fiber 2 also has an influence on m_l, as seen from Figure 13B: a thinner or a longer fiber 2 will decrease the m_l value. Again, using the criterion $m_l \geq 0$, we can find the critical values for D_2 and s_2 to avoid system distortion.

Qualitatively speaking, a higher m_l or a smaller R value will mean a system with more free fibers and fewer bonded areas. This usually leads to a fiber network of less bending stiffness. Figures 12 and 13 can thus serve to improve product performance by choosing fiber 2 with appropriate properties.

MAXIMUM ALLOWABLE FIBER VOLUME FRACTION V_f

Inequality 91 defines the maximum allowable total fiber volume fraction. Again, for an isotropic system where $I = 2/\pi$, Figure 14 gives the relationship of this total fiber volume fraction and some of the important variables. For instance, when the diameter of fiber 2 is given, less fiber volume fraction will be allowed when its length is longer, *i.e.,* when s_2 is greater, according to Figure 14A. Again, this prediction is not influenced by the relative fiber ratio V_2. The effect of D_2 is similar to the case of the R parameter: there is also a critical level of s_2 in Figure 14B. A thicker fiber 2 could result in either a greater or a smaller value or could even have no effect at all on V_{fm}, depending on the s_2 level.

SYSTEM TENSILE MODULUS AND ITS COMPONENTS

Figure 15 shows the relationships between the total fiber volume fraction V_f and the system tensile modulus $E_{jj}, j = 1$ and 2. As expected, increasing V_f will greatly

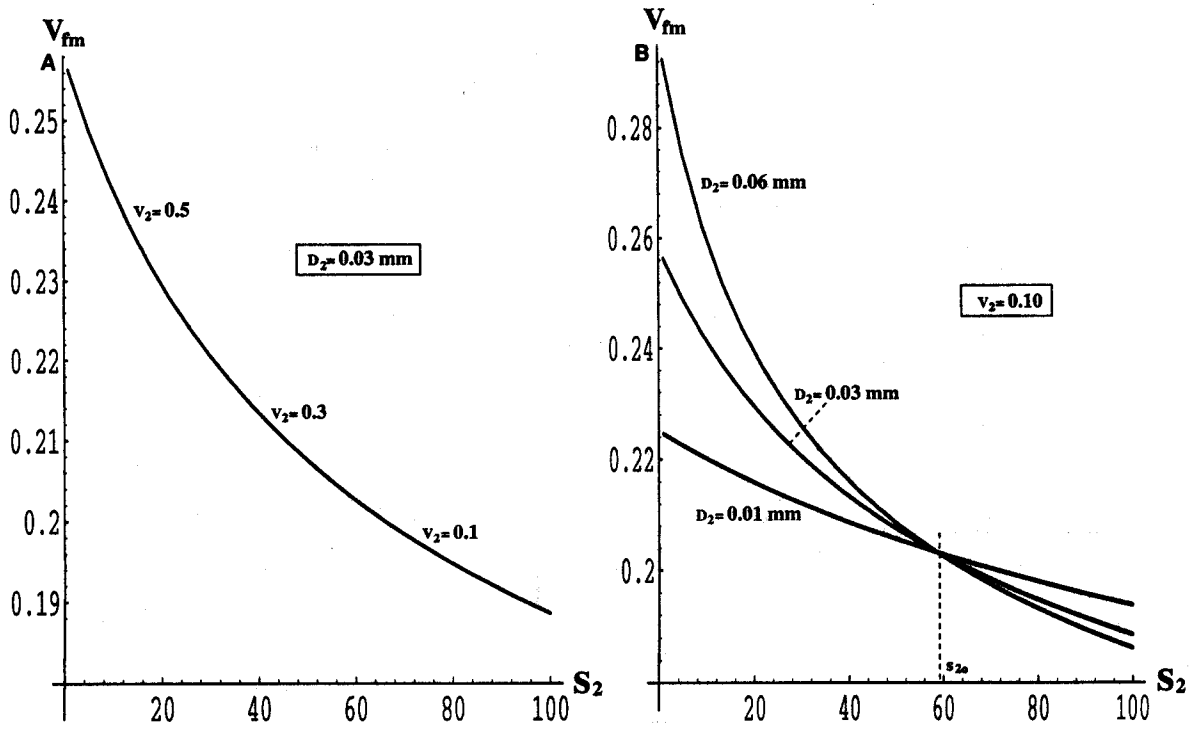

FIGURE 14. Allowable maximum fiber volume fraction V_{fm} value and fiber type 2 properties: (A) V_{fm} versus the fiber aspect ratio s_2 at three levels of fiber volume fraction ratio V_2, and (B) V_{fm} versus the fiber aspect ratio s_2 at three levels of fiber diameter D_2.

increase the system tensile modulus. We can also obtain a higher system tensile modulus by increasing the relative ratio of fiber 2, V_2, in Figure 15. We can prove that a similar result of increased E_{jj} can also be achieved by using a smaller diameter D_2, or a greater s_2, or a higher tensile modulus E_{f2} of fiber type 2.

We have also found through calculations that fiber volume fraction and fiber size are more important factors in determining the system tensile modulus than the fiber tensile modulus itself. That is why increasing the amount of fiber 2 in Figure 15 will augment the system modulus, even though the fiber moduli $E_{f2} < E_{f1}$.

Figure 16 shows the three components of the system tensile modulus. As indicated in Equation 73, the total system tensile modulus is the result of a series system consisting of three components, associated with fiber bending represented by E_{jj}', fiber extension by E_{jj}'', and deformation of the bonded portions by E_{jj}'''. The modulus components associated with fiber deformation, including bending and extension, rely heavily on the total fiber volume fraction V_f and the aspect ratio s_2; a higher V_f or s_2 value leads to greater values for both E_{jj}' and E_{jj}'', as seen in Figures 16A and B. Yet, V_f has no net effect on E_{jj}''', and a higher s_2 value actually reduces E_{jj}''', as shown in Figure 16B. Comparing the magnitudes of the three components, E_{jj}'' and E_{jj}''' are far greater than the value of E_{jj}'. Because of the nature of a series system like Figure 11, at small system strain level, the overall system tensile modulus E_{jj} is largely determined by the much smaller component E_{jj}' or by the effect of fiber bending.

SYSTEM POISSON'S RATIO AND ITS COMPONENTS

The system Poisson's ratio ν_{jr}, j, $r = 1$ or 2, $j \neq r$, as a whole remains constant as revealed in Equation 81, when the effect of the fiber Poisson's ratio itself is ignored. However, the three components that form ν_{jr} do vary, depending on the related parameters. From Equation 75, ν_{jr} is the sum of the three parts—the part associated with fiber bending deformation ν_{jr}', with fiber extension ν_{jr}'', and with bond deformation ν_{jr}'''. In general and under normal conditions, ν_{jr}' is far greater than ν_{jr}'' and ν_{jr}''', as shown in Figure 17, so that $\nu_{jr} \approx \nu_{jr}'$. There are some special cases, however. For instance, when the total fiber volume fraction V_f is at the critical level approaching the maximum allowable value in Figure 17A, ν_{jr}' will become negative, whereas ν_{jr}''' jumps up to a higher value, and ν_{jr}'' with a smaller magnitude compares with the other two but also resonates when $V_f \rightarrow V_{fm}$. The fraction ratio V_2 has significant effects on the three Poisson's ratio compo-

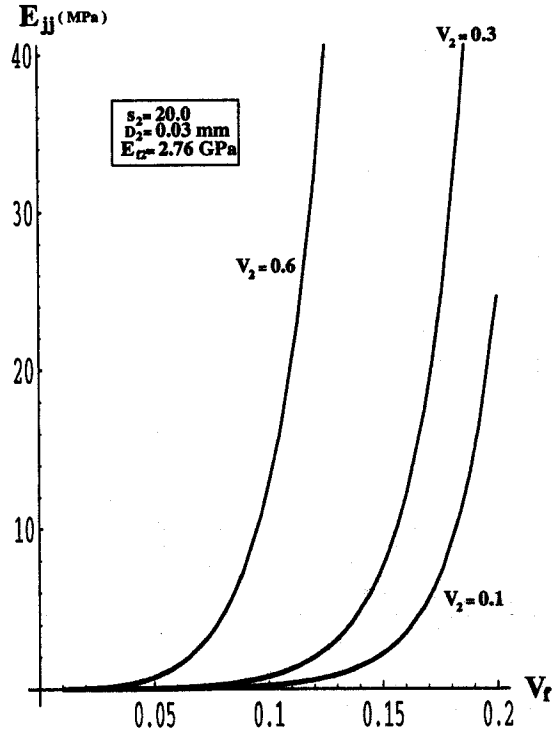

FIGURE 15. E_{jj} versus V_f at three levels of fiber volume fraction ratio V_2.

nents, as shown in Figure 17B. The influences of D_2 and s_2 are marginal, and the tensile modulus E_{f2} of fiber 2 has no effect on any one of the three components and hence no effect on the system Poisson's ratio.

In general, as these results show, the system modulus and Poisson's ratio for small strains are largely determined by the mechanism of fiber bending, and fiber extension and bond deformation are the secondary factors. However, the relative contributions of the three deformation mechanisms can be altered by properly adjusting the amount of fiber 2 added, as well as its properties.

Conclusions

In a fibrous network, there is a fundamental relationship between the fiber orientation parameter I, the fiber dimensional parameter R, and the total fiber quantity V_f, as represented by the inequality

$$IRV_f < \left(\frac{\pi}{8}\right) ,$$

meaning that all three values cannot be determined independently. Because of this interconnection, for a given fibrous system, *i.e.*, with given values for I and R, there is a maximum fiber volume fraction:

$$V_{fm} < \left(\frac{\pi}{8IR}\right) .$$

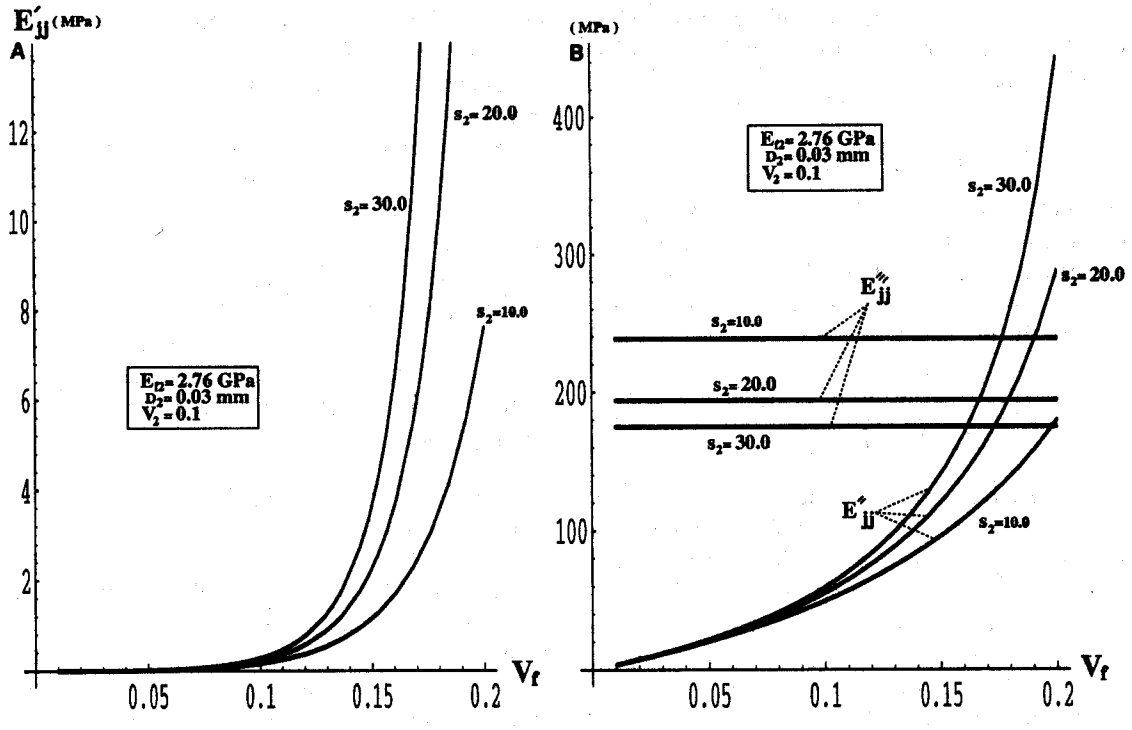

FIGURE 16. Components of system tensile modulus and fiber volume fraction V_f: (A) E_{jj}' versus V_f at three levels of fiber aspect ratio s_2, and (B) E_{jj}'' and E_{jj}''' versus V_f at three levels of fiber aspect ratio s_2.

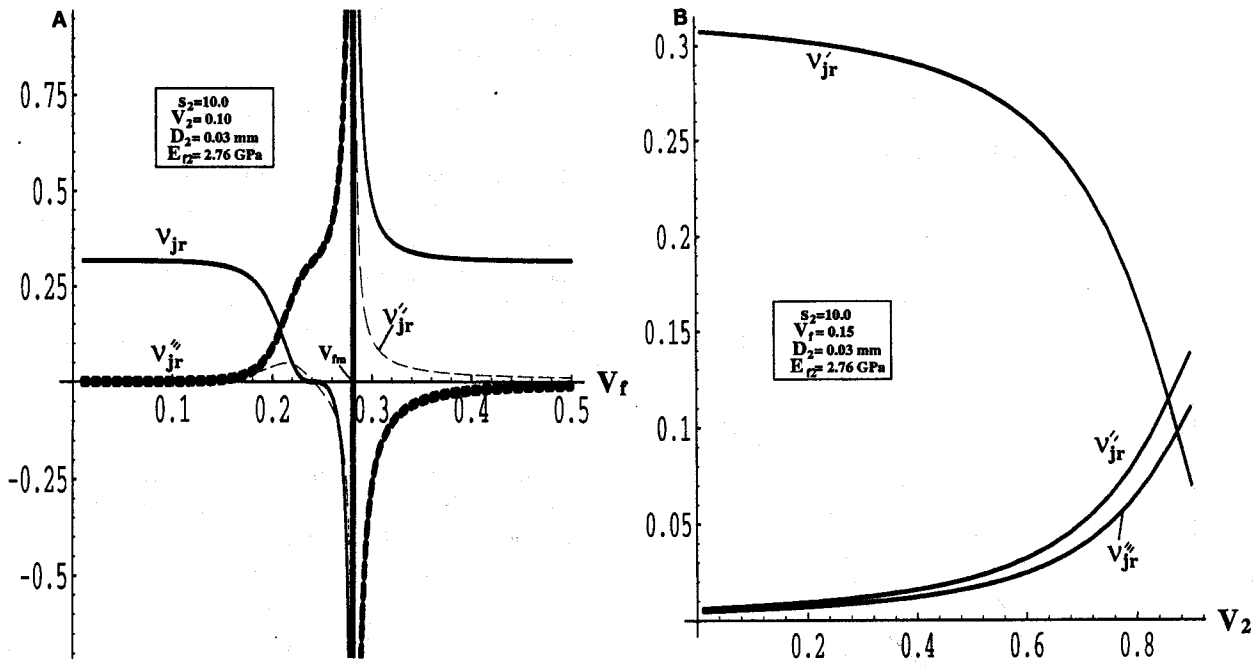

FIGURE 17. Components of system Poisson's ratio versus important parameters: (A) components of the system Poisson's ratio versus V_f, and (B) components of the system Poisson's ratio versus V_2.

Exceeding V_{fm}, the system will be distorted, that is, multiple fibers instead of just two will overlap to form a multilayered nonplanar structure.

The fiber bond area will significantly change the nature of a fibrous system. This effect is reflected by the effective fiber volume fraction,

$$V_{fe} = \frac{V_f}{m_l} = \frac{\pi V_f}{\pi - 8RIV_f} \quad ,$$

which indicates that due to fiber bonding, the system behaves as if there were more fibers than there really are. For instance, in a random fiber orientation case where $I = 2/\pi$ with $V_f = 0.1$, assuming a normal value of $R = 3$, the difference is

$$\frac{V_{fe}}{V_f} = \frac{1}{1 - 0.3\left(\frac{4}{\pi}\right)^2} = 1.9468 \quad .$$

That is, the effective fiber volume fraction has increased by almost 100%. Therefore, for a random system with high fiber volume fraction, it is desirable even for a nonbonding fibrous system to take the fiber contact effect into account. In general, a system with higher effective fiber volume fraction V_{fe} will show a higher deformation resistance so as to influence the performance of the final products. Therefore, proper control of V_{fe} by monitoring the parameters m_l and R can be a way to improve product quality.

Deformation due to fiber bending plays a dominant role in determining both the system modulus and the Poisson's ratio. Fiber elongation and bond deformation only contribute a marginal portion. The relative ratios of these three parts can be modified by changing the amount of the reinforcing fiber and adjusting the fiber properties.

The system modulus is related to many factors such as the total fiber volume fraction, the properties and sizes of the two fiber types, and their relative proportions. Fiber volume and size are more important factors for determining the system tensile modulus than the fiber tensile modulus itself. The overall system Poisson's ratio, on the other hand, is always a constant, although its three components vary mainly with the total fiber volume fraction V_f and the fiber volume fraction ratio V_2.

ACKNOWLEDGMENTS

We would like to thank the Fibers Department of the E.I. DuPont de Nemours & Company for providing financial and technical support for this work and for the guidance and encouragement of staff members Dr. Don Shiffler and Dr. Frank Looney. Thanks are also due the Westvaco Company and staff member Dr. Robert Beran.

Literature Cited

1. Axelrad, D. R., "Micromechanics of Solids," Elsevier Scientific Publishing, NY, 1978.
2. Axelrad, D. R., The Mechanics of Discrete Media, in "Continuum Models of Discrete Systems," E. Kroner and K. H. Anthony, Eds., University of Waterloo Press, 1980, p. 3.
3. Carnaby, G. A., and Pan, N., Theory of the Compression Hysteresis of Fibrous Assemblies, *Textile Res. J.* **59,** 275 (1989).
4. Chen, C. C., and Duckett, K. E., The Direction Distribution on Cross-Contacts Points in Anisotropic Fiber Assemblies, *Textile Res. J.* **49,** 379 (1979).
5. Corte, H., and Kallmes, O., Statistical Geometry of a Fibrous Network, in "Formation and Structure of Paper," vol. 1, F. Bolom, Ed., Tech. Sect. Brit. Papers and Board Makers Assn., London, 1962, p. 13.
6. Cox, H. L., The Elasticity and Strength of Paper and Other Fibrous Materials, *Br. J. Appl. Phys.* **3,** 72 (1952).
7. Jayne, B. A., Some Mechanical Properties of Wood Fibers in Tension, *Forest Prod. J.* **10,** 316 (1960).
8. Kallmes, O., A Comprehensive View of the Structure of Paper, in "Theory and Design of Wood and Fiber Composite Materials," B. A. Jayne, Ed., Syracuse University Press, NY, 1972, p. 157.
9. Kallmes, O., and Corte, H., The Structure of Paper, I: The Statistical Geometry of an Ideal Two-dimensional Fiber Network, *Tappi* **43,** 737 (1960).
10. Kallmes, O., and Bernier, G., The Structure of Paper, IV: The Bonding States of Fibers in Randomly Formed Papers, *Tappi* **46,** 493 (1963).
11. Kallmes, O., Corte, H., and Bernier, G., The Structure of Paper, V: The Free Fiber Length of a Multiplanar Sheet, *Tappi* **46,** 108 (1963).
12. Komori, T., and Makishima, K., Numbers of Fiber-to-Fiber Contacts in General Fiber Assemblies, *Textile Res. J.* **47,** 13 (1977).
13. Komori, T., and Makishima, K., Estimation of Fiber Orientation and Length in Fiber Assemblies, *Textile Res. J.* **48,** 309 (1978).
14. Komori, T., and Makishima, K., Geometrical Expressions of Spaces in Anisotropic Fiber Assemblies, *Textile Res. J.* **49,** 550 (1979).
15. Lee, D. H., Initial Compressional Behavior of a Fiber Assembly (in Korean), Doctoral thesis, Seoul National University, 1985.
16. Lee, D. H., and Lee, J. K., Initial Compressional Behavior of a Fiber Assembly, "Objective Measurement: Applications to Product Design and Process Control," S. Kawabata, R. Postle, and M. Niwa, Eds., The Textile Machinery Society of Japan, Osaka, 1985, pp. 613.
17. Nissan, A. H., and Batten, G. L., Jr., On the Primacy of the Hydrogen Bond in Paper Mechanics, *Tappi* **73,** 159 (1990).
18. Page, D. H., Seth, R. S., and De Grace, J. H., The Elastic Modulus of Paper, I: The Controlling Mechanisms, *Tappi* **62,** 99 (1979).
19. Page, D. H., Seth, R. S., and De Grace, J. H., The Elastic Modulus of Paper, II: The Importance of Fiber Modulus, Bonding, and Fiber Length, *Tappi* **63,** 113 (1980).
20. Page, D. H., El-Hosseiny, F., Winkler, K., and Lancaster, A. P. S., Elastic Modulus of Single Wood Pulp Fibers, *TAPPI* **60,** 114 (1977).
21. Page, D. H., A Theory for the Tensile Strength of Paper, *Tappi* **52,** 674 (1969).
22. Pan, N., and Carnaby, G. A., Theory of the Shear Deformation of Fibrous Assemblies, *Textile Res. J.* **59,** 285 (1989).
23. Pan, N., and Carnaby, G. A., The Initial Shear Modulus of a Unit Cell of Wool Fibers, WRONZ Communication no. C106, 1988.
24. Perkins, R. W., and Ramasubramanian, M. K., Concerning Micromechanics Models for the Elastic Behavior of Paper, in "Mechanics of Cellulosic and Polymeric Materials", R. W. Perkins, Ed., The American Society of Mechanical Engineering, NY, 1989, p. 23.
25. Perkins, R. W., On the Mechanical Response of Materials with Cellular and Finely Layered Internal Structure, in "Theory and Design of Wood and Fiber Composite Materials," B. A. Jayne, Ed., Syracuse University Press, NY, 1972, p. 97.
26. Postle, R., Carnaby, G. A., and de Jong, S., "The Mechanics of Wool Structures," Ellis Horwood Limited, Chichester, U.K., 1988.
27. Ramasubramanian, M. K., and Perkins, R. W., Computer Simulation of the Uniaxial Elastic-Plastic Behavior of Paper, *Trans. ASME* **110,** 117 (1988).
28. Rigdahl, M., Andersson, H., Westerlind, B., and Hollmark, H., Elastic Behaviour of Low Density Paper Described by Network Mechanics, *Fiber Sci. Technol.* **19,** 127 (1983).
29. Schulgasser, K., On the In-Plane Elastic Constants of Paper, *Fiber Sci. Technol.* **15,** 257 (1981).
30. Seth, R., and Page, D. H., The Stress-strain Curve of Paper, in "Proc., The Role of Fundamental Research in Papermaking, 7th Fundamental Research Symposium," Mechanical Engineering Publication, Edmunds, U.K., 1981.

Manuscript received July 29, 1996; accepted February 10, 1997.